Appl. Phys. A 79, 977–981 (2004)
DOI: 10.1007/s00339-004-2607-0

Applied Physics A
Materials Science & Processing

D.S. IVANOV
L.V. ZHIGILEI✉

Combined atomistic-continuum model for simulation of laser interaction with metals: application in the calculation of melting thresholds in Ni targets of varying thickness

Department of Materials Science & Engineering, University of Virginia,
Charlottesville, VA 22904-4745, USA

Received: 2 October 2003/Accepted: 22 January 2004
Published online: 26 July 2004 •

ABSTRACT The threshold laser fluence for the onset of surface melting is calculated for Ni films of different thicknesses and for a bulk Ni target using a combined atomistic-continuum computational model. The model combines the classical molecular dynamics (MD) method for simulation of non-equilibrium processes of lattice superheating and fast phase transformations with a continuum description of the laser excitation and subsequent relaxation of the conduction band electrons based on the two-temperature model (TTM). In the hybrid TTM-MD method, MD substitutes the TTM equation for the lattice temperature, and the diffusion equation for the electron temperature is solved simultaneously with MD integration of the equations of motion of atoms. The dependence of the threshold fluence on the film thickness predicted in TTM-MD simulations qualitatively agrees with TTM calculations, while the values of the thresholds for thick films and bulk targets are $\sim 10\%$ higher in TTM-MD. The quantitative differences between the predictions of TTM and TTM-MD demonstrate that the kinetics of laser melting as well as the energy partitioning between the thermal energy of atomic vibrations and energy of the collective atomic motion driven by the relaxation of the laser-induced pressure should be taken into account in interpretation of experimental results on surface melting.

PACS 61.80.Az; 64.70.Dv; 02.70.Ns

1 Introduction

Short-pulse laser irradiation of a metal target can induce a range of non-equilibrium processes, from strong overheating and fast melting to an explosive boiling and massive material removal (ablation). Experimental analysis of the mechanisms and kinetics of ultrafast laser-induced phase transformations can be performed with optical, X-ray, or electron diffraction time-resolved pump–probe techniques [1–6], whereas the extent of irreversible laser damage can be examined by ex-situ characterization of the target [7–9].

A reliable interpretation of experimental observations requires a solid understanding of the fast non-equilibrium processes occurring in the target material irradiated by a short laser pulse. For short, pico- and femtosecond laser pulses, when the time of the laser energy deposition is comparable or less than the time needed for electron–phonon thermalization, the method of choice in the majority of theoretical/computational investigations is the so-called two-temperature model (TTM) [10]. TTM describes the time evolution of the lattice and electron temperatures by two nonlinear differential equations coupled by a term responsible for the energy exchange due to the electron–phonon coupling.

Despite the successful applications and popularity of TTM, the inherent limitation of the model is its inability to adequately describe the kinetics of phase transformations occurring under highly nonequilibrium conditions induced in the target material by short pulse laser irradiation. In order to overcome this limitation, we are developing a hybrid computational model that combines the MD method for simulation of lattice superheating and fast phase transformations with a continuum TTM description of the laser excitation and subsequent relaxation of the conduction band electrons. The first applications of the TTM-MD model have provided insights into the microscopic mechanisms of laser melting and disintegration of Ni and Au films [11, 12], photomechanical spallation of bulk Ni targets [13], as well as disintegration and ablation of Cu targets [14]. The hybrid model was also used in a recent study of shock-induced heating and melting of a grain boundary region in an Al crystal [15].

In this paper we report the results of the application of the TTM-MD model for investigation of the onset of short pulse laser melting in Ni films of different thicknesses and a bulk Ni target. Irradiation parameters are chosen to match the ones used in a recent experimental investigation [1]. The threshold laser fluences for the onset of surface melting are calculated with TTM-MD model and compared to the prediction of the conventional TTM model. Implications of the simulation results for interpretation of experimental data are discussed.

2 Combined TTM-MD model

In the combined model the MD method completely substitutes the TTM equation for the lattice temperature. The diffusion equation for electron temperature, T_e, is solved by a finite difference method simultaneously with MD integra-

✉ Fax: +1-434/982-5660, E-mail: lz2n@virginia.edu

tion of the equations of motion of atoms,

$$\text{TTM: } C_\mathrm{e}(T_\mathrm{e})\frac{\partial T_\mathrm{e}}{\partial t} = \nabla(K_\mathrm{e}(T_\mathrm{e}, T_\mathrm{l})\nabla T_\mathrm{e}) - G(T_\mathrm{e} - T_\mathrm{l}) + S(z, t) \tag{1}$$

$$\text{MD:} \quad m_i \frac{\mathrm{d}^2 \boldsymbol{r}_i}{\mathrm{d}t^2} = \boldsymbol{F}_i + \xi m_i \boldsymbol{v}_i^T \,,$$

$$T_\mathrm{l}^\mathrm{cell} = \sum_{i=1}^{N^\mathrm{cell}} m_i (\boldsymbol{v}_i^T)^2 \Big/ (3k_\mathrm{B} N^\mathrm{cell}) \tag{2}$$

where in (1) C_e is the electron heat capacity, K_e is the electron thermal conductivity, G is the electron–phonon coupling constant, and the source term $S(z, t)$ is used to describe the local laser energy deposition per unit area and unit time during the laser pulse duration. In (2), m_i and r_i are mass and position of an atom i, F_i is the force acting on atom i due to the interatomic interactions. An additional term, $\xi m_i \boldsymbol{v}_i^\mathrm{T}$, is added to the ordinary MD equations of motion to account for the electron–phonon coupling. The cells in the finite difference discretization are related to the corresponding volumes of the MD system and the local lattice temperature, $T_\mathrm{l}^\mathrm{cell}$, is calculated for each cell from the average kinetic energy of the thermal motion of atoms. Thermal velocity of an atom i is defined as $\boldsymbol{v}_i^\mathrm{T} = \boldsymbol{v}_i - \boldsymbol{v}^\mathrm{c}$, where $\boldsymbol{v}_i$ is the actual velocity of the atom, and $\boldsymbol{v}^\mathrm{c}$ is the velocity of the center of mass of a cell to which atom i belongs. The coefficient ξ in the coupling term is calculated for each cell at each MD integration time step and is designed to ensure the energy conservation in the electron-lattice system. The expansion, density variations, and, at higher fluences, disintegration of the irradiated target predicted in the MD part of the model are accounted for in the continuum part of the model. A complete description of the combined TTM-MD model is given elsewhere [12].

The hybrid approach, briefly described above, combines the advantages of the two-temperature model and the MD method. The two-temperature model provides an adequate description of the laser energy absorption into the electronic system, energy exchange between the electrons and phonons, and fast electron heat conduction in metals, whereas the MD method is appropriate for simulation of non-equilibrium processes of lattice superheating, melting, and ablation.

In this work we apply the TTM-MD model to study the dependence of the threshold fluence for surface melting on the film thickness. Simulations are performed for free-standing Ni films of four different thicknesses, 30 nm, 50 nm, 75 nm, and 100 nm, as well as for a bulk Ni target. The initial MD computational cell is an FCC crystal with lateral dimensions of 3.53×3.53 nm. The number of atoms in the computational cell is 34 000 atoms in 30 nm film, 56 800 atoms in 50 nm film, 85 200 atoms in 75 nm film, and 113 600 atoms in 100 nm film. Periodic boundary conditions are applied in the lateral directions, parallel to (100) free surface(s). In the case of a bulk sample, the MD method is used only in the top 100 nm of the target, whereas the diffusion equation for electron temperature is solved in a much wider 600 nm region, providing an adequate representation of the electronic heat conduction into the bulk of the target. In order to avoid reflection of the pressure waves propagating from the irradiated surface, the dynamic boundary condition [16] is applied at the bottom of the MD region. Before applying laser irradiation, all systems are equilibrated at 300 K. Laser pulse duration of 200 fs is used in the simulations and the absorbed laser fluence rather then the incident fluence is used in the discussion of the simulation results.

Thermal and elastic properties of the lattice are defined in the TTM-MD model by the inter-atomic potential, described in this work by the embedded-atom method (EAM) in the form suggested in [17]. The parameters used in the TTM equation for the electronic temperature, (1), are as follows [1, 11, 12], $C_\mathrm{e} = \gamma T_\mathrm{e}$ with $\gamma = 1065\ \mathrm{J\ m^{-3}\ K^{-2}}$, $K_\mathrm{e} = K_0 T_\mathrm{e}/T_\mathrm{l}$ with $K_0 = 91\ \mathrm{Wm^{-1}K^{-1}}$, $G = 3.6 \times 10^{17}\ \mathrm{Wm^{-3}K^{-1}}$. A justification of the choice of the approximation used to describe the dependence of the electron thermal conductivity K_e on the electron and lattice temperatures is given in [12].

3 Results and discussions

Surface melting thresholds predicted in TTM and TTM-MD calculations are shown for Ni targets of different thickness in Fig. 1a. To compare the results of TTM-MD and TTM calculations, the parameters of the model EAM Ni material are used in the TTM equation for the lattice temperature. A series of constant pressure–constant temperature simulations was performed to determine the equation of state of the EAM Ni material, whereas the melting temperature was found in liquid-crystal coexistence MD simulations. The equilibrium melting temperature at zero pressure, T_m, is found to be 1439 K, the latent heat of melting, H_m, is $2.17 \times 10^9\ \mathrm{J\ m^{-3}}$, the value of the heat capacity at constant pressure, c_p, increases from $4.08 \times 10^6\ \mathrm{J\ m^{-3}\ K^{-1}}$ at 300 K to $5.32 \times 10^6\ \mathrm{J\ m^{-3}\ K^{-1}}$ at T_m. The temperature dependence of the lattice heat capacity obtained from MD simulations was approximated by a polynomial function and used in TTM calculations presented in Fig. 1a.

In order to make our conclusions usable for quantitative interpretation of experimental data, we also performed TTM calculations with experimental parameters for Ni, $T_\mathrm{m} = 1728$ K, $H_\mathrm{m} = 2.45 \times 10^9\ \mathrm{J\ m^{-3}}$ [18], and $c_\mathrm{p} = 4.1 \times 10^6\ \mathrm{J\ m^{-3}\ K^{-1}}$ [1]. The results of these calculations are shown in Fig. 1b [19].

To define the melting threshold in a TTM-MD simulation, we arbitrary choose the condition at which the number of atoms in the liquid phase corresponds to that in a 2 nm layer in the initial crystal before the irradiation. In Fig. 1a, the two graphs calculated by TTM correspond to the fluences at which the melting temperature is reached at the very surface of the target (solid line) and the fluences at which the total amount of the melted material in the target is equivalent to a 2 nm layer (dashed line). The melting process is included into TTM calculation by a simple assumption that as soon as the melting temperature is reached in a given cell of the finite difference discretization, all the additional energy supplied to the lattice by the heat conduction and transferred from the hot electrons through the electron–phonon coupling goes to the latent heat of melting until all the material in the cell is melted. An alternative to this crude approximation would be to allow overheating and to include a description of the kinetics of laser melting based on the classical nucleation theory, e.g., [20]. Recent MD simulations of laser melting [11, 12]

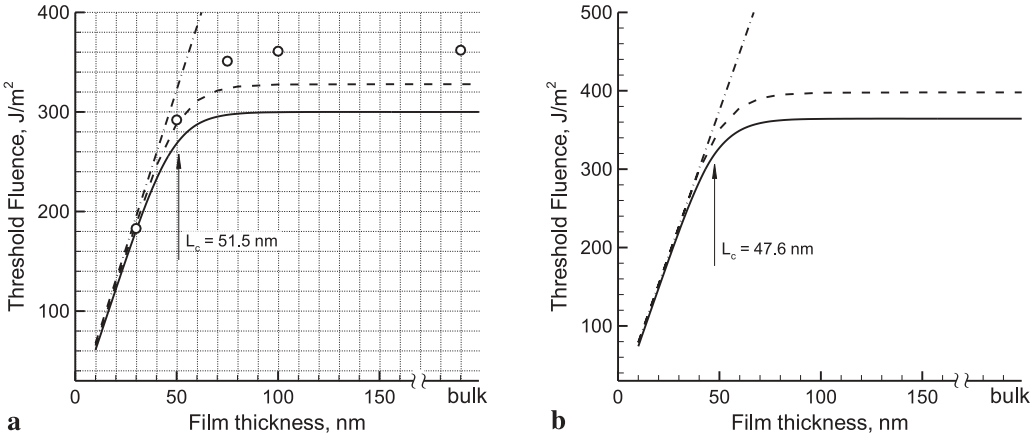

FIGURE 1 Surface melting threshold versus film thickness calculated with the combined TTM-MD model (*data points*) and TTM model (*dashed* and *solid lines*) for laser irradiation with 200 fs laser pulses. The data points for the TTM-MD simulations in **a** and the *dashed line* for the TTM calculations show the fluences at which the maximum amount of the melted material corresponds to a 2 nm layer in the original target. The *solid line* shows the fluence at which the melting temperature is reached at the very surface of the target, as predicted by TTM. The *dash-dotted line* corresponds to the energy needed to homogeneously heat the whole film up to the melting temperature and melt 2 nm region of the film. Properties of the model EAM Ni material are used in TTM calculations in **a**, experimental properties of Ni [1] are used in **b** [19]

suggest, however, that relaxation of the laser-induced stresses can result in anisotropic deformation of the surface region and reduction of the overheating required for the initiation of the homogeneous melting down to almost zero. Therefore, in this work we decide to not include overheating into the TTM calculations. Note that both overheating and the effect of the relaxation of the laser-induced stresses are naturally included in the TTM-MD model, which does not require any a priori assumptions on the lattice response to the fast laser heating.

As we can see from Fig. 1a, both TTM-MD and TTM models predict nearly linear increase of the threshold fluence with film thickness up to a certain thickness, L_c, that corresponds to the diffusive penetration depth of the excited electrons before the electron–phonon equilibration at the threshold for melting. The value of L_c can be estimated following the method proposed in [21] and the results of the estimation are shown by arrows in Fig. 1 [19]. In films thinner than L_c, nearly uniform temperature distributions are established by the time of electron–phonon equilibration. As a result, the threshold fluences for laser melting are defined by the energy density needed to homogeneously heat the film up to the melting temperature and melt a 2 nm layer of the film (dash-dotted lines in Fig. 1). The maximum depths of melting at the front and back surfaces of a 30 nm film are found to be approximately equal to each other, whereas the maximum amount of melted material at the back surface of a 50 nm film accounts only for $\sim 10\%$ of the total amount of the liquid phase. For films thicker than L_c, the electron–phonon equilibration takes place within the electronic diffusion length L_c from the irradiated surface, melting is observed at the front surface only, and the threshold fluence saturates and approaches the value characteristic for a bulk target.

While both TTM-MD and TTM predict similar dependences of the melting threshold from the film thickness, the threshold values obtained in TTM-MD model for films with thickness significantly above L_c are $\sim 10\%$ higher as compared to the ones predicted by TTM. To explain this discrepancy, we have to consider the kinetics of the melting process occurring under conditions of the fast laser energy deposition as well as additional channels for partitioning of the deposited energy, not accounted for in TTM but present in a more realistic TTM-MD model.

The kinetics of energy redistribution in a TTM-MD simulation of a partial laser melting of a 100 nm Ni film irradiated by a 1 ps laser pulse is illustrated in Fig. 2. The fluence of $430\,\mathrm{J/m^2}$ is chosen in this simulation so that the maximum depth of the melted surface region would reach ~ 15 nm. A larger, as compared to the simulations discussed above, depth of melting allows us to better illustrate, in addition to other channels of the laser energy partitioning, the energy transfer to the latent heat of melting. Following the energy deposition by a 1 ps laser pulse, the total energy is conserved for the rest of the simulation. Initially all the laser energy is deposited into the energy of electrons, E_e. The electron–phonon coupling leads to the fast, within ~ 20 ps, transfer of more than a half of the deposited laser energy to the thermal en-

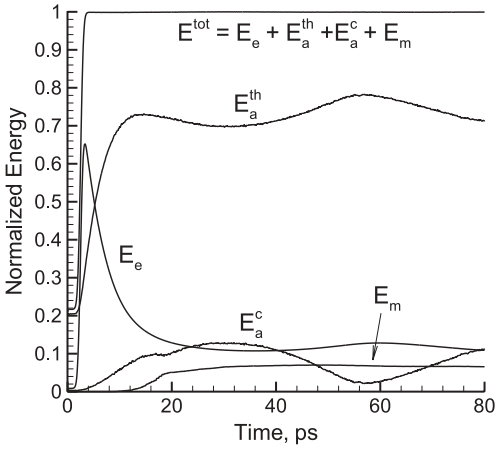

FIGURE 2 Energy partitioning in a 100 nm Ni film irradiated with a 1 ps laser pulse at an absorbed fluence of $430\,\mathrm{J/m^2}$. The thermal energies of the electrons, E_e, and the atoms, E_a^{th}, the energy of the collective atomic motion due to the elastic vibrations of the film, E_a^c, the energy transferred to the latent heat of melting, E_m, and the total energy of the system, E^{tot}, are shown. Energies are normalized to the total energy absorbed by the film

ergy of the atomic motion, E_a^{th}. The fast temperature increase leads to the buildup of a compressive pressure in the irradiated film. The relaxation of the initial pressure induces a collective atomic motion of the elastic vibrations of the film. The energy of the elastic vibrations, E_a^c, includes contributions of the kinetic and potential energies associated with the collective atomic motion in the film. E_a^c also includes a smaller static component due to a contribution from anisotropic thermoelastic stresses that cannot relax by the uniaxial expansion of the film in the direction normal to the surface. These static anisotropic stresses remain in the crystalline part of the target even after the relaxation of the elastic oscillations of the film [13].

The time dependence of the energy of melting, E_m, reflects the kinetics of the melting process. The energy spent on melting is determined by multiplying the fraction of the liquid phase in the system by the latent heat of melting of the model material. The fraction of the liquid phase is calculated based on the local order parameter defined in [12]. In the simulation illustrated by Fig. 2, a fast homogeneous melting of ~ 11 nm surface region of irradiated film is followed by a slower heterogeneous melting of additional 4 nm of the film by liquid-solid front propagation.

As we can see from Fig. 2, the energy transferred from the excited electrons to the lattice splits into three parts, the energy of the thermal motion of the atoms, E_a^{th}, the energy of melting, E_m, and the energy of the collective atomic motion associated with the relaxation of the laser-induced stresses, E_a^c. The latter part is not accounted for in a simple TTM model. The energy of the collective motion of atoms can be comparable (up to $\sim 15\%$ in Fig. 2) to the energy of the thermal motion of atoms and should be taken into account in the analysis of the energy density needed to melt the material. Two additional factors are found to have a strong effect on the melting process. First, the material can be significantly (up to $\sim 20\%$ [12]) overheated above its equilibrium melting temperature when the time of the laser heating (defined by the laser pulse duration and/or the time of electron–phonon equilibration, whichever is longer) is shorter than the time needed for the melting front propagation from the free surface(s) of the target. Second, the fast relaxation of the laser-induced pressure can only proceed in the direction normal to the surface of the target, leading to the uniaxial expansion and associated anisotropic lattice distortions. The anisotropic deformation of the film reduces the lattice stability against the initiation of melting. As a result, the overheating required for the initiation of homogeneous melting can be reduced down to less then $T \approx 1.05 T_m$ [11]. The net results of all the factors described above is that the thresholds for laser melting of sufficiently thick films predicted in the TTM-MD simulations are $\sim 10\%$ higher as compared to the ones obtained in TTM calculations.

Although the effects of the overheating and laser-induced collective atomic motion described above are present in films of any thickness, for films thinner or comparable with the electronic diffusion length L_c, we observe a good agreement between the predictions of TTM and TTM-MD models. This observation is related to the kinetics of the laser melting process. In a thick film or a bulk target, a fast transient melting of a surface region is followed by recrystallization, whereas in a film thinner than L_c the lattice heating proceeds almost homogeneously throughout the film and the melted parts of the film remains melted at later times (surface melting is detected at both sides of films thinner than L_c and the melting depths at the front and back sides become closer to each other as the film thickness decreases). The predictions of both TTM and TTM-MD calculations for films thinner than L_c are, therefore, close to the straight dash-dotted lines in Fig. 1 that correspond to the homogeneous heating of the whole film and permanent melting of a surface region(s). An important difference between the TTM and TTM-MD simulations, however, is that the melting of thin films (30 nm and 50 nm) takes much longer in the TTM-MD simulations, as shown in Table 1. As discussed above and illustrated in Fig. 2, in TTM-MD simulations a significant part of the deposited laser energy goes to the nonthermal energy of the elastic oscillations of the film. Gradual dissipation of the oscillations, occurring on the timescale of hundreds of picoseconds, leads to the energy transfer from the energy of the collective atomic motion, E_a^c, to the energy of the thermal motion of the atoms, E_a^{th}, Fig. 2. In a thin film homogeneously heated up to the melting temperature, the energy transferred from E_a^c to E_a^{th} is further transferred to the latent heat of melting, E_m, leading to a gradual advancement of the melting front. As a result, the melting process in films thinner than L_c takes much longer in TTM-MD simulations as compared to TTM simulations that do not include a description of the thermoelastic material response to the fast laser heating, Table 1.

Thickness (nm)	Time of the maximum melting depth (ps)	
	TTM	TTM-MD
30	50	~750
50	18	~750
75	15	40
100	13	38
bulk	13	34

TABLE 1 Time when the maximum melting depth of 2 nm is reached in TTM and TTM-MD simulations of surface melting of Ni films of different thickness and a bulk Ni target irradiated with a 200 fs laser pulse. For 30 nm films no recrystallization of the melted regions is observed and the times shown in the table correspond to the saturation in the time dependence of the amount of melted material

4 Summary

In summary, the quantitative differences between the predictions of TTM and TTM-MD demonstrate that the kinetics of laser melting as well as the energy partitioning between the thermal and collective atomic motions induced by the fast laser energy deposition should be taken into account in interpretation of the experimental results on surface melting.

ACKNOWLEDGEMENTS The authors would like to thank Dr. B. Rethfeld of Universität Essen for insightful comments and discussions and Dr. J. Güdde of the Philipps-Universität Marburg for helpful communication at the final stage of the paper preparation.

REFERENCES

1 S.-S. Wellershoff, J. Hohlfeld, J. Güdde, E. Matthias: Appl. Phys. A **69**, S99 (1999)

2 M.B. Agranat, S.I. Ashitkov, V.E. Fortov, A.V. Kirillin, A.V. Kostanovskii, S.I. Anisimov, P.S. Kondratenko: Appl. Phys. A **69**, 637 (1999)
3 B. Lin, H.E. Elsayed–Ali: Surf. Sci. **498**, 275 (2002)
4 K. Sokolowski-Tinten, C. Blome, J. Blums, A. Cavalleri, C. Dietrich, A. Tarasevich, I. Uschmann, E. Förster, M. Kammler, M. Horn-von-Hoegen, D. von der Linde: Nature **422**, 287 (2003)
5 B.J. Siwick, J.R. Dwyer, R.E. Jordan, R.J.D. Miller: Science **302**, 1382 (2003)
6 O.P. Uteza, E.G. Gamaly, A.V. Rode, M. Samoc, B. Luther-Davies: in preparation.
7 S. Preuss, A. Demchuk, M. Stuke: Appl. Phys. A **61**, 33 (1995)
8 T.D. Bennett, C.P. Grigoropoulos, D.J. Krajnovich: J. Appl. Phys. **77**, 849 (1995)
9 M. Hashida, A.F. Semerok, O. Gobert, G. Petite, Y. Izawa, J.F. Wagner: Appl. Surf. Sci. **197**–**198**, 862 (2002)
10 S.I. Anisimov, B.L. Kapeliovich, T.L. Perel'man: Sov. Phys. JETP **39**, 375 (1974)
11 D.S. Ivanov, L.V. Zhigilei: Phys. Rev. Lett. **91**, 105 701 (2003)
12 D.S. Ivanov, L.V. Zhigilei: Phys. Rev. B **68**, 064 114 (2003)
13 E. Leveugle, D.S. Ivanov, L.V. Zhigilei: Appl. Phys. A, in press
14 C. Schäfer, H.M. Urbassek, L.V. Zhigilei: Phys. Rev. B **66**, 115 404 (2002)
15 D.S. Ivanov, L.V. Zhigilei, E.M. Bringa, M. De Koning, B.A. Remington, M.J. Caturla, S.M. Pollaine: Proceedings of APS Topical Conference on Shock Compression of Condensed Matter, in press (2003)
16 L.V. Zhigilei, B.J. Garrison: Mat. Res. Soc. Symp. Proc. **538**, 491 (1999)
17 X.W. Zhou, H.N.G. Wadley, R.A. Johnson, D.J. Larson, N. Tabat, A. Cerezo, A.K. Petford-Long, G.D.W. Smith, P.H. Clifton, R.L. Martens, T.F. Kelly: Acta Mater. **49**, 4005 (2001)
18 *CRC Handbook of Chemistry and Physics*, 72nd edition, ed. by D.R. Lide, (CRC Press, Boca Raton, FL 1991)
19 Due to a minor difference in the definition of the diffusive penetration depth of excited electrons used in this work and in [1, 21], the value of L_c is larger by a factor of $2^{5/8}$ as compared to the one reported in [1]. A more significant quantitative discrepancy is observed between the results of TTM calculations reported in [1] and the results presented in Fig. 1b of this paper. In particular, the saturation fluences at which the melting temperature is reached at the surface of thick Ni samples is $220\,\mathrm{J/m^2}$ in [1] (Fig. 8b) and $363\,\mathrm{J/m^2}$ in our calculations (Fig. 1b). This discrepancy is due to a mistake in the TTM code used in [1], as identified through private communication with one of the authors of [1], Dr. J. Güdde. New test calculations performed by Dr. Güdde and Dr. Rethfeld agree with the data presented in this paper.
20 B. Rethfeld, K. Sokolowski-Tinten, D. von der Linde, S.I. Anisimov: Phys. Rev. B **65**, 092 103 (2002)
21 P.B. Corkum, F. Brunel, N.K. Sherman, T. Srinivasan-Rao: Phys. Rev. Lett. **61**, 2886 (1988)